SUBSURFACE STRUCTURE EVOLUTION ASSOCIATED WITH THE RISE AND FALL OF INTENSELY ACTIVE REGIONS

Richard. S. Bogart[1], Sarbani Basu[2], Maria Cristina Rabello-Soares[1], and H. M. Antia[3]

[1]*Stanford University, Stanford, CA 94305-4085, USA*
[2]*Astronomy Department, Yale University, New Haven CT 06520-8101, USA*
[3]*Tata Institute of Fundamental Research, Homi Bhabha Road, Mumbai 400005, India*

ABSTRACT

In order to study the sub-surface structure variations associated with the formation and evolution of major active regions producing large, long-lived sunspot groups and intense flare activity, we analyze the localized power spectra at the sites of selected active regions from well before their emergence through their disappearance, comparing the helioseismic data with those for quiet regions of the same size and at the same latitude during similar time ranges. Because of the need for continuous data through disc passages of the selected regions over several Carrington rotations, we have analyzed GONG Doppler data, for which nearly continuous observations are always available, whereas continuous MDI data are usually limited to two rotations or less. The studied active regions were selected from among those that attained the greatest sunspot group area during the years for which there is reasonably complete GONG+ data coverage, from the middle of 2001 through 2005.

Key words: local helioseismology; active region evolution.

1. INTRODUCTION

Earlier studies of the sub-surface structure of highly-developed active regions have revealed significant differences from the structure of the quiet sun at depths of 2–15 Mm below the photosphere, the region best resolved with local ring-diagram analysis. In order to better understand the processes associated with the formation and evolution of such active regions, we would like to be able to apply the same analysis techniques to the areas in which they exist over the course of their lifetimes. Intense active regions usually give rise to long-lived sunspot groups, typically enduring at the surface for two or three Carrington rotations. We would thus like to be able to track the same regions for at least four or five rotations, from before the emergence of magnetic activity visible at the surface through the return to quiet-sun conditions, along with consistently quiet regions at the same latitude during similar time ranges. Because of the need for continuous data through disc passages of the selected regions over several Carrington rotations, we have analyzed GONG Doppler data, for which nearly continuous observations are always available, whereas continuous MDI data are usually limited to two rotations or less. The studied active regions were selected from among those that attained the greatest sunspot group area during the years for which there is reasonably complete GONG+ data coverage, from the middle of 2001 through 2005.

Since ring-diagram analysis has proven successful when the observational duty cycle is high, we require periods of nearly continuous data over four or more rotations, or at least those parts of the rotations when the active region site is crossing the visible disc. Such data coverage at a spatial resolution suitable for ring-diagram analysis is only available from the GONG+ network. We have thus restricted our study to major active regions that formed during the years for which there is reasonably complete GONG+ data coverage, *i.e.* from the middle of 2001 through 2005. During this time period, there were 18 NOAA active regions that attained a maximum spot group area of at least 1000 millionths; these are listed in Table 1. Since new region numbers are assigned whenever existing regions appear at the east limb, some of these regions correspond to others during later or earlier disc passages. For example, AR 10488 was clearly the same as AR 10507 and 10525 in the two following rotations, and AR 10808 was the same as AR 10798 in a preceding rotation. Of the regions in Table 1, however, only AR 10036, 10069, and 10105 are associated with the same physical region, one that had a sunspot area exceeding 1000 millionths during three consecutive rotations.

For this study we focus on two of these large active regions, AR 10488 and 10808, the 3rd and 7th largest in the sample. They both existed in areas relatively free from other activity. AR 10488 first appeared on the visible hemisphere, grew rapidly, had a comparatively simple bipolar structure at maximum, and decayed gradually over about three rotations; it also crossed central meridian close to disc centre. AR 10808 first appeared as a small group at the east limb in a previous rotation (as 10798) and was already in decline as it appeared in its primary rotation. A low level of activity persisted at its location

Table 1. Active regions with spot group area > 1000*: 2001.06.01–2005.12.31.*

AR #	First Seen	Lat	Lon	Last Seen	Lat	Lon	AMax	(rank)
9608	2001.09.05	-24	112	2001.09.18	-30	094	1110	13
9682	2001.10.25	9	172	2001.11.06	13	170	1210	11
9690	2001.11.05	-18	026	2001.11.18	-17	017	1420	8
9742	2001.12.15	9	217	2001.12.28	12	213	1070	14
9934	2002.05.01	-18	212	2002.05.14	-15	211	1060	16
10030	2002.07.09	18	017	2002.07.22	20	006	1350	9
10036	2002.07.15	-7	296	2002.07.27	-8	297	1070	14
10069	2002.08.11	-8	297	2002.08.24	-8	298	1990	2
10105	2002.09.07	-6	301	2002.09.20	-7	299	1520	6
10162	2002.10.17	25	134	2002.10.31	26	113	1120	12
10349	2003.04.26	-14	154	2003.05.07	-14	153	1030	17
10375	2003.06.01	11	023	2003.06.14	12	022	1250	10
10484	2003.10.18	5	351	2003.10.30	1	356	1750	3*
10486	2003.10.22	-16	286	2003.11.04	-17	284	2610	1
10488	2003.10.27	9	292	2003.11.04	8	290	1750	3
10720	2005.01.10	9	177	2005.01.22	11	176	1630	5
10756	2005.04.25	-6	230	2005.05.07	-7	227	1030	17
10808	2005.09.07	-12	229	2005.09.19	-11	232	1430	7

for three subsequent rotations, giving rise to a small complex of short-lived active regions while the center of original activity drifted off to the west (Figure 1).

To quantify the level of magnetic activity, we use the Magnetic Activity Index (MAI), an area integral of the strong field ($|\mathbf{B}| > 50G$) observed by MDI over the same time and spatial region as that over which the Doppler data are tracked. The field strength measured by MDI tends to saturate at a few hundred G. The combination of that effect with the removal of small fields (necessary to avoid rectifying noise), means that the MAI lies somewhere between a measure of the total field strength and the total area covered by strong field. This may account for the peculiar behaviour of the MAI of a region as it crosses the disc, as exhibited in Fig. 2. For weak regions, the MAI is approximately proportional to μ, the cosine of the central angle; but higher values seem to be more nearly proportional to $\mu^{1/2}$. Note especially the behaviour of AR 10507, the second avatar of 10488.

We select three regions at fixed longitudes and at the same latitude, one centred on the site of the target region and the others at consistently quiet locations. We determine the mode power spectra for each region as it crosses disc centre during each Carrington rotation. We then invert the differences in frequencies between the target and comparison regions for the parameters of interest. To first order, this procedure eliminates most of the systematic errors that may arise in ring-diagram analysis due to geometric foreshortening, astigmatism, and mapping/tracking errors.

For AR 10808, we tracked the target and comparison regions for 4096 min centered on the times of their central meridian crossings. For AR 10488 we tracked the regions for 8192 min. We also tracked the AR 10488 regions for five separate 1664-min intervals, separated by 15 degrees of Carrington rotation, and averaged those sets of spectra for each region together. All regions were tracked in mapped circles of diameter 12°.

The ring fitting procedure is as described in Basu *et al.* (2004), with both SOLA (Pijpers & Thompson, 1992; 1994) and RLS inversions of the frequency differences between common modes. We find, surprisingly, that the number of modes fit and useful after weeding for the inversions is practically independent of the level of data coverage (Fig. 4).

2. RESULTS

The differences in mode parameters at the height of activity between an active region and a nearby quiet region are shown in Fig. 6 & 7. They are similar to those seen in studies of other active regions (*cf.* Rajaguru *et al.*, 2001; Basu *et al.*, 2004), with lower amplitudes, greater linewidths, and lower frequencies for fixed wavelengths, particularly at higher frequencies. The trends over time of the differences in amplitude and line-width between the active site and the comparison sites are interesting; they suggest that the disturbances affecting mode propagation persist longer than the relative increase in magnetic ac-

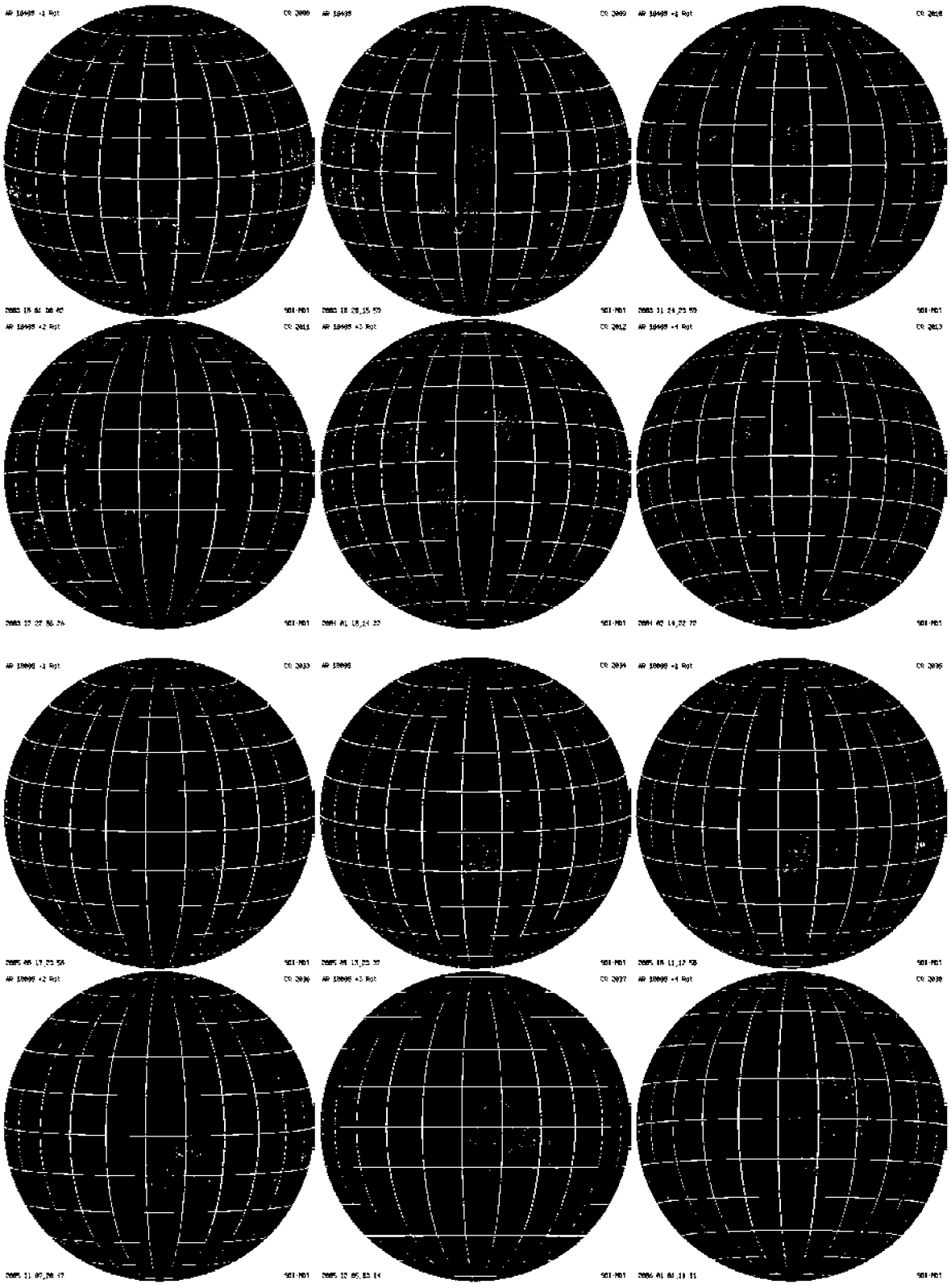

Figure 1. (above) MDI magnetograms centered on the Carrington longitude of AR 10488 ($292°.5$*, latitude* $+07°.5$*) for six successive Carrington rotations. The areas analyzed are* $12°$ *diameter circles centered at this longitude, and comparison quiet regions at longitudes* $215°$ *and* $320°$ *and at the same latitude. The grid is at* $15°$ *spacings. (below) MDI magnetograms centered on the Carrington longitude of AR 10808 (*$230°$*, latitude* $-10°$*) for six successive Carrington rotations. The comparison quiet regions are at longitudes* $200°$ *and* $320°$ *and at the same latitude*

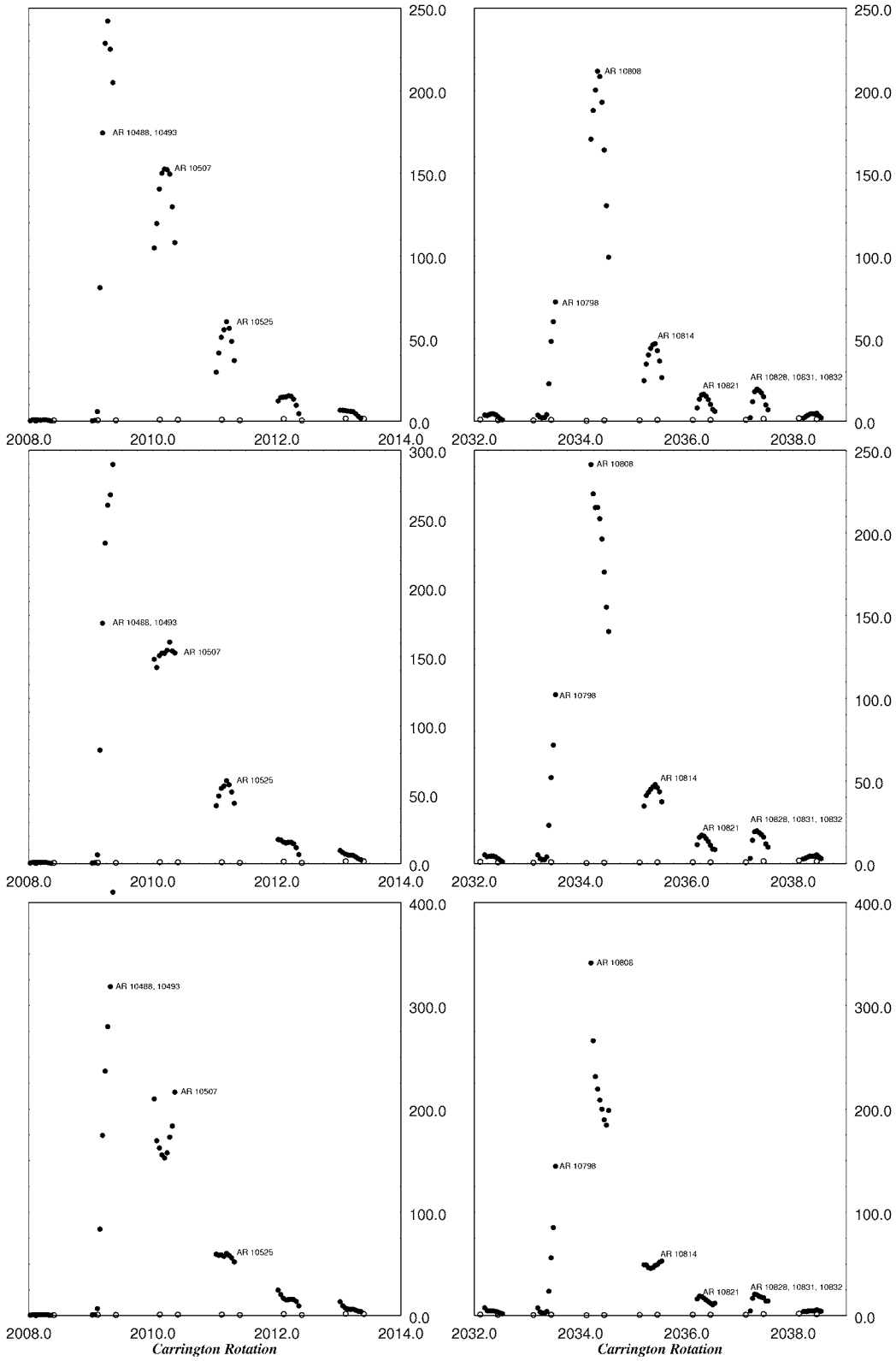

Figure 2. (left) The Magnetic Activity Index (MAI) for the target region AR 10488 at intervals of $15°$ *in solar rotation during each of six successive Carrington rotations. The open circles representing the MAI of the comparison regions are shown only at disc centre. Panel A (top) shows the raw values of MAI; those in Panel B are normalized by* $\cos(\mathrm{lon})^{1/2}$ *and those in panel C (bottom) by* $\cos(\mathrm{lon})$*; central meridian longitude is an approximate proxy for central angle, since the regions are at low latitude. (right) The same, for the target region AR 10808 over seven rotations.*

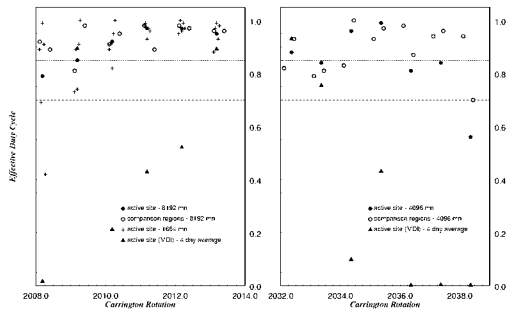

Figure 3. (left) The effective duty cycle of the GONG network during both the 8192-min intervals and single 1664-min intervals over which AR 10488 and its comparison regions were analyzed. MDI data coverage is shown for intervals comparable to the 8192-min ones. (right) The same, for the 4096-min intervals over which AR 10808 and its comparison regions were analyzed

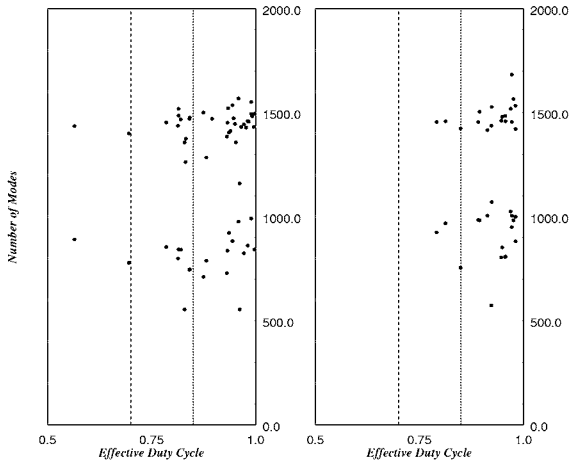

Figure 4. The number of modes fit (before and after weeding in the inversion), as a function of the effective duty cycle, for both 4096-minute intervals (left) and 8192-min inervals (right). Fits for all regions regardless of activity levels are included. Raw mode fit counts are shown in black, weeded ones in blue.

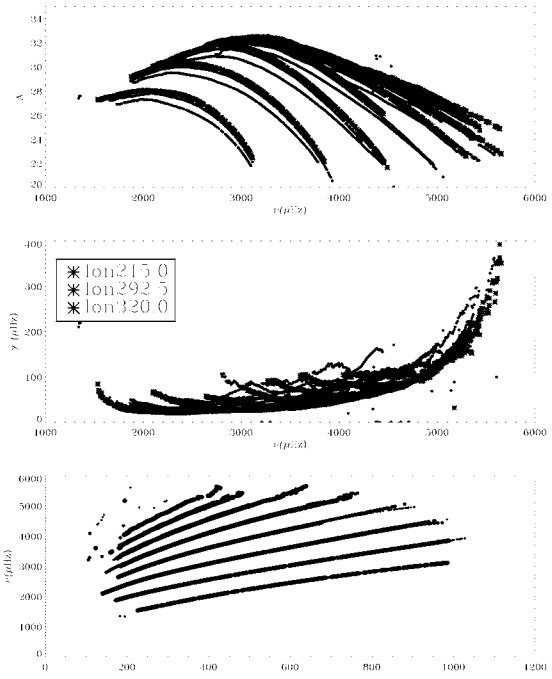

Figure 5. Amplitudes (top), widths (middle) and frequencies of the fitted modes for each of the the three analyzed regions for AR 10488 during CR 2009, the rotation when it appeareed.

tivity, particularly around 3 mHz and 5 mHz, where they exhibit notably different evolutionary behaviour.

Results for inversions of the depth depndence of the differences in the bulk velocity and the sound speed parameters are shown in Figs. 8–10. As suggested by the behaviour of the mode parameters, the largest excursion in the flow pattern seem to occur after the active region has reached its maximum, especially at depth. The sound-speed inversions have proven very difficult so far, and it still too early to draw any conclusions. The largest effects are seen at the time of maximum, but the variation of the thermal depth profiles is not consistent with a simple dependence on activity.

3. CONCLUSIONS

The results presented here are preliminary, and more active regions must be analyzed before we can draw meaningful conclusions. Nevertheless, we have learned some useful facts concerning the data analysis procedure itself, and can at least pose a few tentative findings, to be confirmed by further analysis:

- Inversions of flows from 12 regions at GONG resolution work reasonably well, but sound speed inversions are so far difficult.
- The numbers of invertible modes do not depend

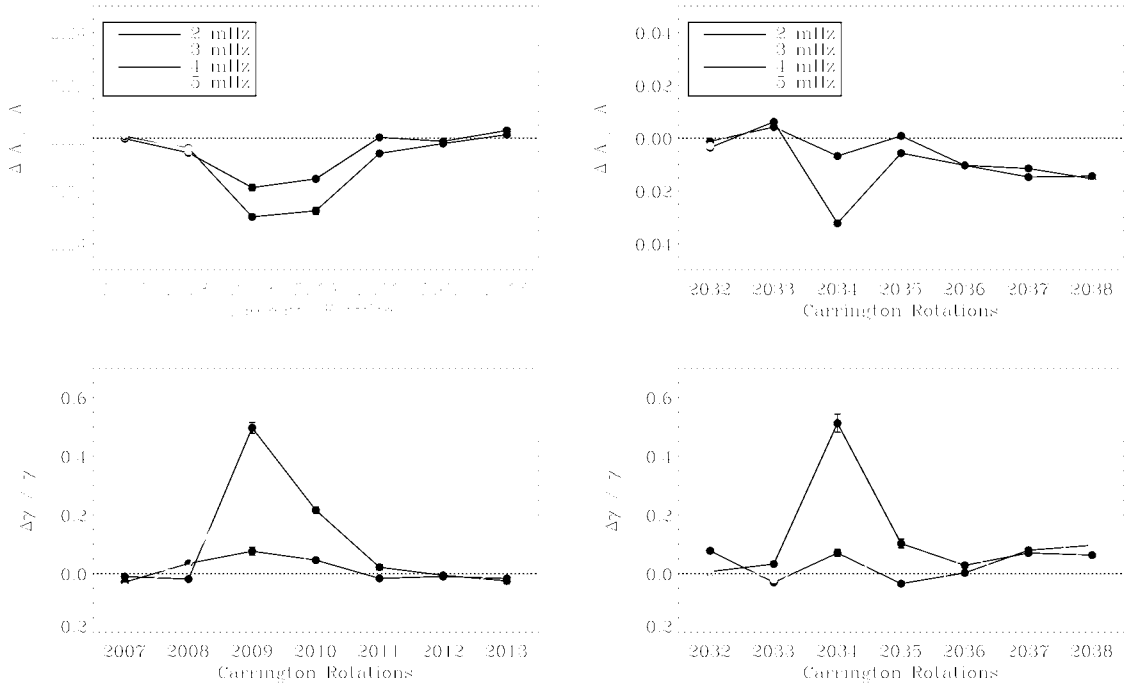

Figure 7. Differences in the average mode amplitudes (top) and widths between the target active regions and the averages of their comparison quiet regions at selected frequencies , as functions of time. The parameters for the regions associated with AR 10488, starting from two rotations before its appearance, are shown on the left; those for 10808 start one rotation before the appearnce of its precursor, but the precursor only appeared near the end of the analysis interval.

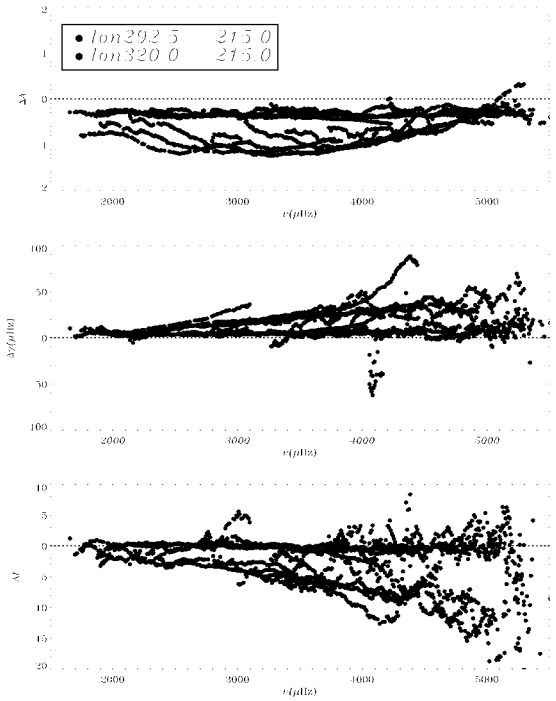

Figure 6. Differences in the mode parameters Amplitude, Width and Frequency of the fitted modes between one of the the quiet comparison regions and the target active region and the other comparison region for AR 10488 during CR 2009.

strongly on the duty cycle, at least down to levels of 0.7.

- The effects on mode amplitudes and lifetimes at activity sites persists well beyond the maxima in activity; this is particularly true around 3 mHz and 5 mHz, but the evolutionary behaviour is quite different at low and high frequencies.
- The flow patterns around the active region sites are most strongly disturbed after the active region has peaked, particularly at depth.
- There is no evidence for precursor behaviour in the mode parameters nor in the inferred flows.
- The Magnetic Activity Index exhibits a central-angle dependence intermediate between that of total flux and filling factor, depending on the level of activity.

ACKNOWLEDGMENTS

This work utilizes data obtained by the Global Oscillation Network Group (GONG) program, managed by the National Solar Observatory, which is operated by AURA, Inc. under a cooperative agreement with the National Science Foundation. The data were acquired by instruments

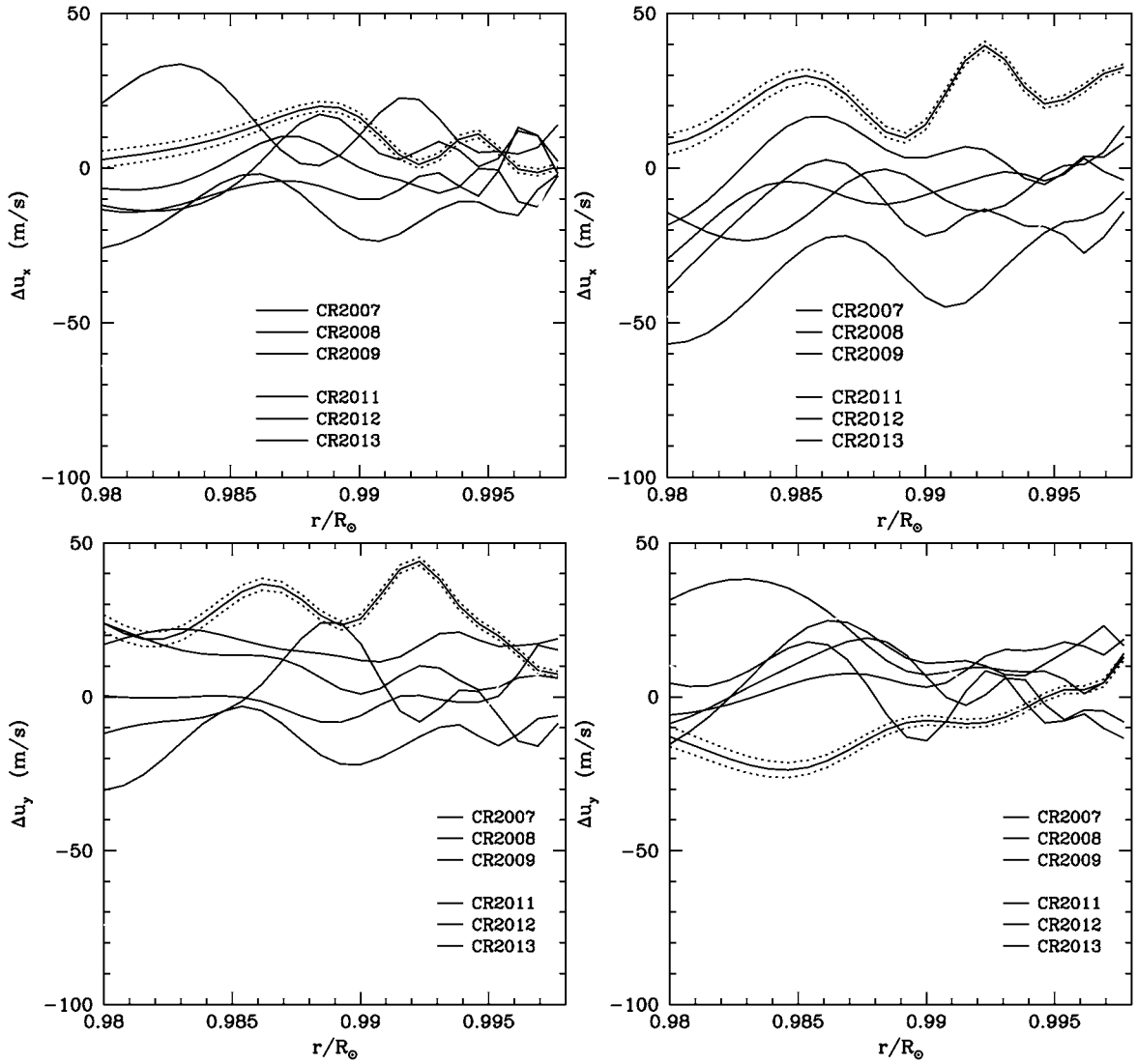

Figure 8. SOLA inversions for the depth dependence of the difference in u_x (above) and u_y between the site of active regions AR 10488 and its comparison regions for each rotation over the course of seven rotations. The inversions are from fits of the averages of five 1664-min tracked spectra during each rotation. The plots on the left show the differences between the active region site and the average of those for the two quiet comparison sites; those on the right show the differences between the two quiet sites. The formal errors are shown for CR 2007, those for other rotations are similar.

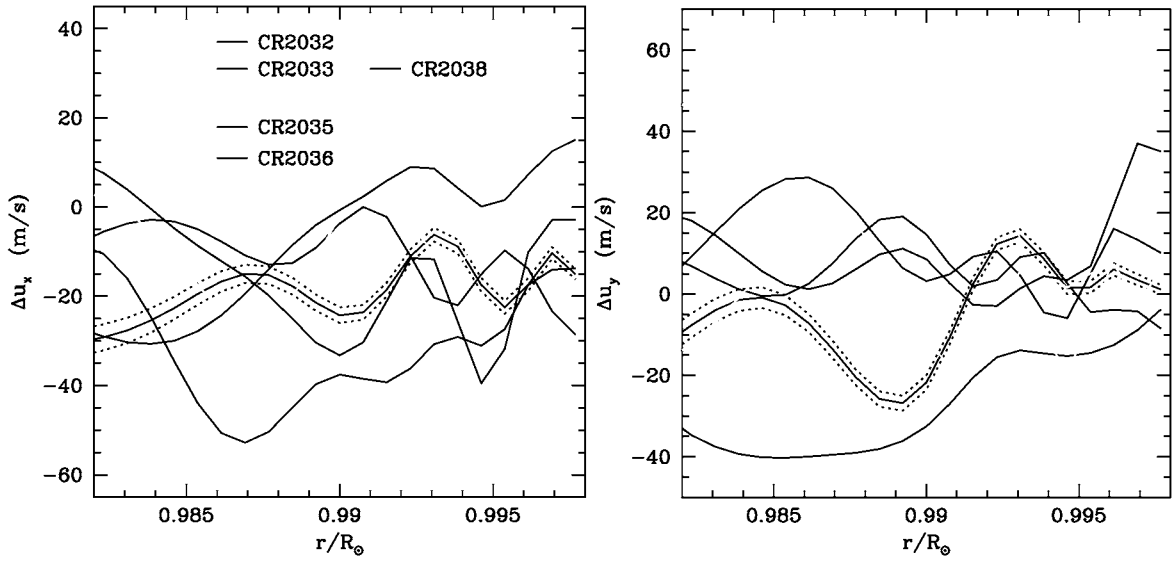

Figure 9. Inversions for the depth dependence of the difference in u_x (left) and u_y between the site of AR 10808 and the average of its comparison regions for each rotation over the course of six rotations. These results are based on fits to spectra for single 4096-min trackings of each region.

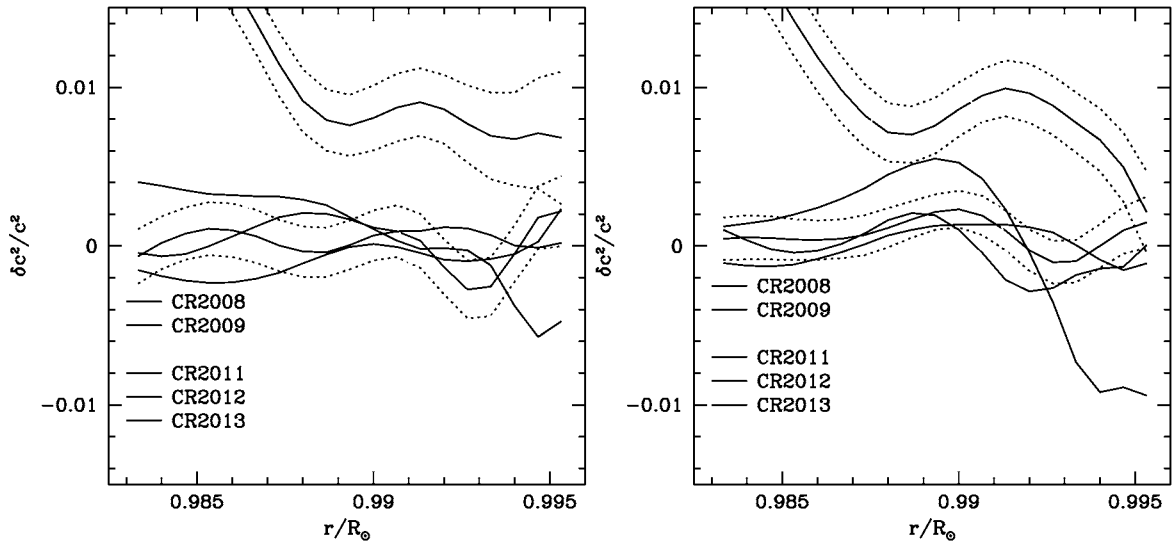

Figure 10. Inversions for the depth dependence of the difference in sound speed (c^2) between the site of AR 10488 and the average of its comparison regions for each rotation over the course of six rotations. The inversions at left are based on fits to spectra for single 8192-min trackings of each region, those at right on averages of five 1664-min trackings.

operated by the Big Bear Solar Observatory, High Altitude Observatory, Learmonth Solar Observatory, Udaipur Solar Observatory, Instituto de Astrofisica de Canarias, and Cerro Tololo Interamerican Observatory. This work s;dp uses data from the Solar Oscillations Investigation / Michelson Doppler Imager (SOI/MDI) on the Solar and Heliospheric Observatory (SOHO). The MDI project is supported by NASA grant NAG5-8878 to Stanford University. SOHO is a project of international cooperation between ESA and NASA. This work was supported by NASA grants NAG5-10912 & NNG06GD13G and by NSF grant ATM-0348837 to SB.

REFERENCES

[1] Basu, S., Antia, H.M., and Bogart, R.S. 2004. Ap.J. **610**, 1157.

[2] Pijpers, F.P. and Thompson, M.J. 1992. A&A **262**, L33.

[3] Pijpers, F.P. and Thompson, M.J. 1994. A&A **281**, 231.

[4] Rajaguru, S. P., Basu, S., and Antia, H.M. 2001. Ap.J. **563**, 410.